Climate Data Record (CDR) Program

Climate Algorithm Theoretical Basis Document (C-ATBD)

AVHRR Aerosol Optical Thickness (AOT)

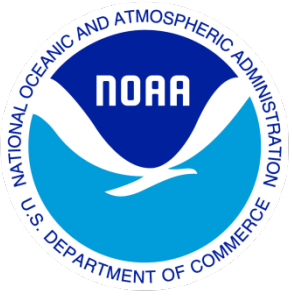

CDR Program Document Number: CDRP-ATBD-0096
Configuration Item Number: 01B-04
Revision 4 /April 12, 2022

REVISION HISTORY

Rev.	Author	DSR No.	Description	Date
1	Xuepeng Zhao, NCEI	DSR-101	Initial Submission to CDR Program	02/24/2011
2	Xuepeng Zhao, NCEI	DSR-477	2nd submission to CDR Program	06/11/2013
3	Xuepeng Zhao, NCEI	DSR-752	3rd submission to REDR (former CDR) Program	07/27/2016
4	Xuepeng Zhao, NCEI	DSR-1612	4th submission to CDR Program	04/12/2022

TABLE of CONTENTS

1. INTRODUCTION 6
1.1 Purpose 6
1.2 Definitions 6
1.3 Referencing this Document 6
1.4 Document Maintenance 7

2. OBSERVING SYSTEMS OVERVIEW 8
2.1 Products Generated 8
2.2 Instrument Characteristics 8

3. ALGORITHM DESCRIPTION 9
3.1 Algorithm Overview 9
3.2 Processing Outline 9
3.3 Algorithm Input 10
3.3.1 Primary Sensor Data 10
3.3.2 Ancillary Data 11
3.3.3 Derived Data 12
3.3.4 Forward Models 12
3.4 Theoretical Description 12
3.4.1 Physical and Mathematical Description 12
3.4.2 Data Merging Strategy 14
3.4.3 Numerical Strategy 14
3.4.4 Calculations 15
3.4.5 Look-Up Table Description 15
3.4.6 Parameterization 16
3.4.7 Algorithm Output 16

4. TEST DATASETS AND OUTPUTS 18
4.1 Test Input Datasets 18
4.2 Test Output Analysis 18
4.2.1 Reproducibility 18
4.2.2 Precision and Accuracy 22
4.2.3 Error Budget 22

5. PRACTICAL CONSIDERATIONS 24
5.1 Numerical Computation Considerations 24
5.2 Programming and Procedural Considerations 24
5.3 Quality Assessment and Diagnostics 24
5.4 Exception Handling 24
5.5 Algorithm Validation 24
5.6 Processing Environment and Resources 26

6. ASSUMPTIONS AND LIMITATIONS 28
6.1 Algorithm Performance 28
6.2 Sensor Performance 28

7. FUTURE ENHANCEMENTS 29
7.1 Enhancement 1 29
7.2 Enhancement 2 29
7.3 Enhancement 3 29

8. REFERENCES 30

APPENDIX A. ACRONYMS AND ABBREVIATIONS 33

LIST of FIGURES

Figure 1: High level flowchart of the AVHRR AOT CDR Retrieval System (AACRS), illustrating the main processing sections. 10

Figure 2: Example of daily orbital AOT (at 0.63μm channel) product for NOAA-16/AVHRR ascending node on January 1, 2005. 19

Figure 3: Example of daily mean AOT (at 0.63μm channel) CDR product for January 1, 2005 by averaging the daily orbital AOT from the AVHRR of NOAA-15, -16, -17, and -18. 19

Figure 4: Example of monthly mean AOT (at 0.63μm channel) CDR product for January 2005 20

Figure 5: Example of AVHRR AOT CDR (0.63μm) time series for the versions 1, 2, and 3 and their comparison with Terra/MODIS AOT (0.55μm). 20

Figure 6: AOT distribution on the north polar latitudes in July 2019 for version 3.0 (left panel) and version 4.0 (right panel). 21

Figure 7: Comparison of global AVHRR AOT CDR (0.63μm) time series between version 3.0 (yellow dashed line) and version 4.0 (blue dashed line) 22

Figure 8: Scatter plots of AVHRR retrievals versus AERONET observations for 0.67μm channel (left panel) and 0.83μm channel (right panel) 25

Figure 9: Scatter plots of AVHRR retrievals (ordinate) versus MAN observations (abscissa) for 0.63μm channel. 26

LIST of TABLES

Table 1: Version tracking for the AVHRR AOT CDR product releases. 7

Table 2: Example of AVHRR channels and the channels selected for aerosol retrieval. Channel 3a is only available for the AVHRR instrument on NOAA-15, -16, -17, -18, -19. 8

Table 3: Primary AVHRR sensor L2B input data for aerosol retrieval. 11

Table 4: Ancillary input data from the AVHRR+HIRS PATMOS-x L2B product and sea ice concentration CDR. 11

Table 5: Look-up table (LUT) input data. 12

Table 6: Microphysical properties of ocean aerosol model used in the AOT algorithm, including geometric mean radius (r_g), standard deviation (σ_g), and refractive index. 13

Table 7: Arguments and dimensions of three LUTs. 16

Table 8: Daily orbital AOT product in HDF format. 16

Table 9: Daily mean CDR AOT product in NetCDF-4 format. 17

Table 10: Monthly mean CDR AOT product in NetCDF-4 format. 17

Table 11: Systematic and random errors for the AVHRR AOT retrieval based on surface AERONET validation. 23

1. Introduction

1.1 Purpose

The purpose of this document is to describe the algorithm submitted to the National Centers for Environmental Information (NCEI) by Xuepeng (Tom) Zhao/NCEI that will be used to create the AVHRR Aerosol Optical Thickness (AOT) Climate Data Record (CDR) (see Chan et al., 2013; Zhao et al., 2013; Zhao et al., 2016), using the NOAA AVHRR+HIRS PATMOS-x Level-2B data product (see Heidinger et al., 2014). The actual algorithm is defined by the computer program (code) that accompanies this document, and thus the intent here is to provide a guide to understanding that algorithm, from both a scientific perspective and in order to assist a software engineer or end-user performing an evaluation of the code.

1.2 Definitions

Following is a summary of the symbols used to define the algorithm.

Spectral and directional parameters:

$$\lambda = \textit{wavelength of retrieval channels.} \quad (1)$$

$$\theta_s = \textit{solar zenith angle.} \quad (2)$$

$$\theta_v = \textit{view zenith angle.} \quad (3)$$

$$\phi_{sv} = \textit{relative azimuth angle.} \quad (4)$$

$$\eta = \textit{glint angle.} \quad (5)$$

Atmospheric parameters:

$$\tau = \textit{aerosol optical thickness.} \quad (6)$$

$$\rho = \textit{reflectance} \quad (7)$$

1.3 Referencing this Document

This document should be referenced as follows:

AVHRR Aerosol Optical Thickness (AOT) - Climate Algorithm Theoretical Basis Document, NOAA Climate Data Record Program CDRP-ATBD-0096 Rev. 4 (2022). Available https://www.ncei.noaa.gov/products/climate-data-records/avhrr-aerosol-optical-thickness

1.4 Document Maintenance

Table 1 describes the versions of the AVHRR AOT CDR product releases with their corresponding software package and the C-ATBD versions.

Table 1: Version tracking for the AVHRR AOT CDR product releases.

Product Version	Software Version	C-ATBD Revision	Release Data	Remarks
v01r00	v01r00	1.	02-24-2011	Initial Release
v02r00	v02r00	2.	06-11-2013	2nd Submission
v03r00	v03r00	3.	07-27-2016	3rd Submission
V04r00	V04r00	4.	04-12-2022	4th Submission

For the AOT versions 1 (v01r00) product, the resampled pixel level clear-sky reflectance of AVHRR PATMOS-x version 5/revision 1 (v05r01) is used as the input for the AOT CDR production. The AOT CDR product is in 1^{o}x1^{o} equal angle grid. For the AOT version 2 (v2r00) product, the Level-2B clear-sky reflectance of AVHRR PATMOS-x version 5/revision 2 (v05r02) in 0.1^{o}x0.1^{o} orbital grid is used as the input for the AOT CDR production. New thresholds for selecting better clear-sky reflectance and reducing cloud contamination have been implemented in the AOT version 2 production and the product is delivered in 0.1^{o}x0.1^{o} equal angle grid. For version 3 (v03r00), the Level-2B clear-sky reflectance of AVHRR PATMOS-x version 5/revision 3 (v05r03) in 0.1^{o}x0.1^{o} orbital grid is used as the input for the AOT CDR production. For version 4 (v04r00), the Level-2B clear-sky reflectance of AVHRR + HIRS PATMOS-x version 6/revision 0 (v06r00) in 0.1^{o}x0.1^{o} orbital grid is used as the input for the AOT CDR production. Cloud detection and screening are further improved in the input data so that cloud contamination is further reduced in the AOT CDR version 4, which is in 0.1^{o}x0.1^{o} equal angle grid. Both versions 1 and 2 are static delivery but versions 3 and 4 will be forward updated every quarter. Version 4/revision 0 (v04r00) is also used to replace version 3 (v03r00) for forward updated every quarter.

2. Observing Systems Overview

2.1 Products Generated

The objective of this algorithm is to retrieve the aerosol optical thickness (AOT) from NOAA operational AVHRR sensor (such as NOAA-14) orbital grids at selected spatial (such as 0.1x0.1 degree) and temporal (such as 1 time per day) resolution in cloud free condition during daytime. The final product is also in 0.1^{o}x0.1^{o} equal angle grid (total 1800 x 3600 = 6480000 grids over the globe). Due to the relatively large uncertainties associated with surface reflectance over water glint area and land surface as well as limited AVHRR retrieval channels, the current algorithm only performs retrieval over non-glint water surface (specifically at the anti-solar side of the orbit and viewing angle is larger than 40^{o} away from the specular ray). The primary retrieval product is AOT at 0.63μm. However AOT at 0.83μm (or 1.61μm) is also retrieved for consistent check purpose. Thus, only the AOT at channel 1 (or 0.63μm) is output as the CDR product, which is in NetCDF-4 format.

2.2 Instrument Characteristics

The aerosol products will be generated for each cloud-free orbital grid (0.1^{o} x 0.1^{o}) of AVHRR re-sampled imager from pixel level (~4km x 5km) AVHRR imager. The aerosol retrieval makes use of 2 to 3 channels from visible to near-infrared bands depending on a specific AVHRR sensor and its available channels (Table 2 is an example for AVHRR instrument) where aerosol signal is relatively strong but gas absorption is weak. The channels used for detecting unfavorable retrieval conditions (such as over land) are still under investigation; therefore, the channels used in current algorithm are subject to change as development continues.

Table 2: Example of AVHRR channels and the channels selected for aerosol retrieval. Channel 3a is only available for the AVHRR instrument on NOAA-15, -16, -17, -18, -19.

Channel number	Wavelength (μm)	Aerosol retrieval over water
1	0.63	X (AOT)
2	0.83	X (AOT)
3a	1.61	X (AOT)
3b	3.75	
4	11.0	
5	12.0	

3. Algorithm Description

3.1 Algorithm Overview

This is the complete description of the algorithm at the current level of maturity (which will be updated with each revision). The algorithm is developed for aerosol retrieval over ocean only since SWIR channel (e.g., 2.13μm) required generally for the aerosol retrieval over land is not available from AVHRR instrument. The retrieval is first performed on daily orbital grids, then, the products are averaged to produce daily mean and monthly mean products. The aerosol retrieval algorithm provides estimates of aerosol optical thickness (AOT or τ) in the visible (0.63μm) and near infrared (0.83μm or 1.61μm) channels of AVHRR instrument (Zhao et al., 2004, 2008, 2013), assuming the molecular atmosphere, aerosol microphysics, and surface reflectance are known. In practice, the relationship between aerosol optical thickness, τ, and dimensionless top-of-atmosphere (TOA) apparent reflectance, ρ, (radiance normalized to solar flux at the top of the atmosphere) is described by a 4-dimensional lookup table (LUT), pre-calculated for different τ, solar and viewing geometries using the 6S radiative transfer model (Vermote et al., 1997a,b). The clear-sky reflectances of AVHRR in channel 1 (0.63μm) and 2 (0.83μm) or 3a (1.61μm) are input to the retrieval scheme. The clear-sky is defined as the cloudy probability (cpb) is less than and equal to 1% (or cpb ≤1%). The cpb for a grid is determined from 3x3 grids around it by using a naïve Bayesian cloud detection technique (see Heidinger et al., 2012). Aerosol optical thickness (τ_1 and τ_2) are retrieved independently from both channels. For this reason the algorithm is described as an "independent" two-channel algorithm. A weak absorbing aerosol model and a bimodal log-normal size distribution are used in the 6S code for the generation of LUTs. Other parameters specified as input to the LUTs are Lambertian oceanic reflectance with diffuse glint correction to the aerosol phase function. Detailed explanation of this aerosol retrieval algorithm is presented in the following sections.

3.2 Processing Outline

The processing outline of the AVHRR AOT CDR Retrieval System (AACRS) is summarized in the Figure 1, which includes the basic sections as input, output, and aerosol retrievals over water. The algorithm to create aerosol product is written in IDL. Input data is PATMOS-x AVHRR+HIRS level-2B (L2B) product in NetCDF format and output daily orbital product in HDF format are served as an intermediate product, which is further averaged to produce daily mean and monthly mean grided products in NetCDF format (version 4). Only the daily and monthly mean products serve as the CDR products and will be distributed for public assess by NCEI.

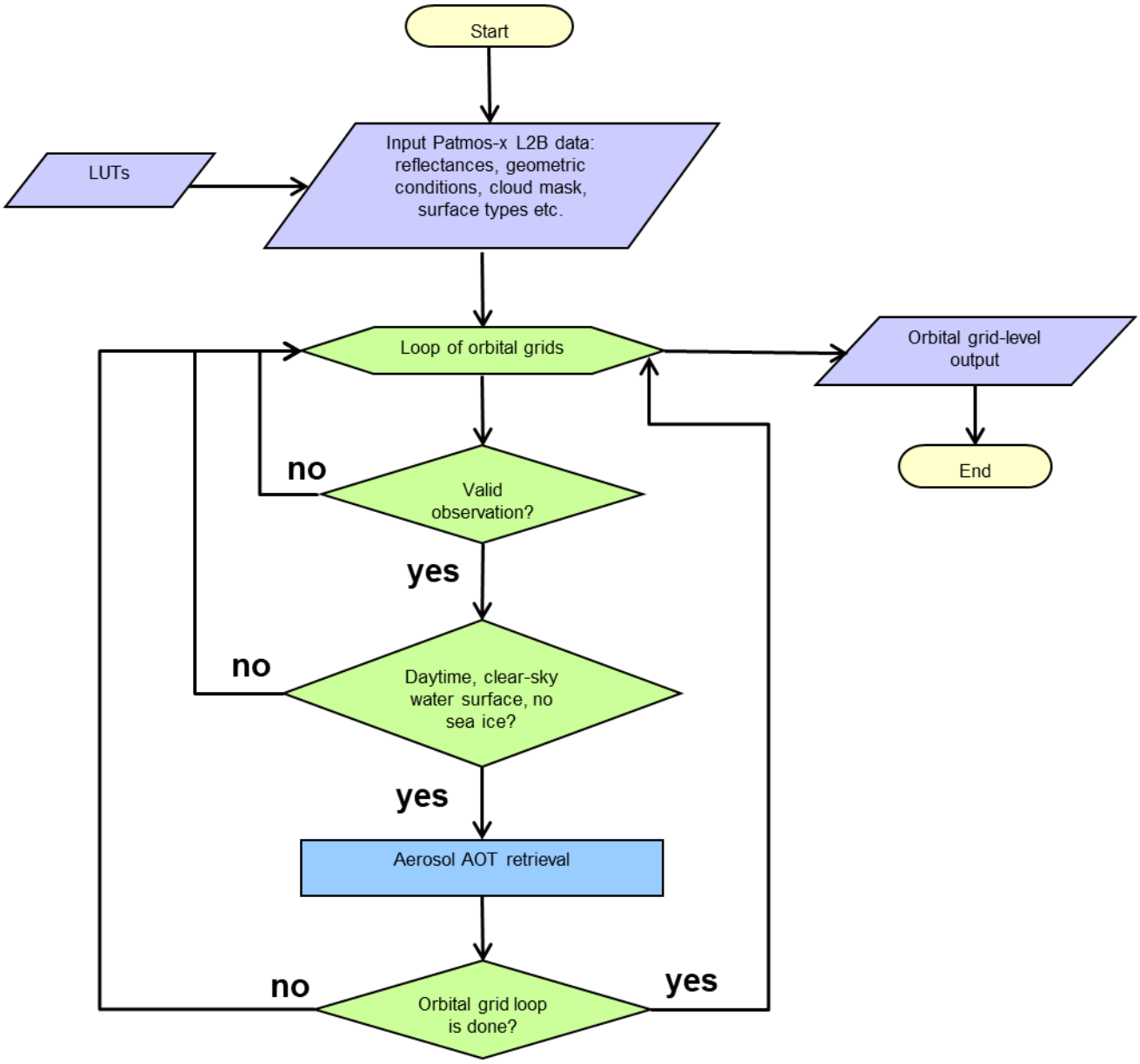

Figure 1: High level flowchart of the AVHRR AOT CDR Retrieval System (AACRS), illustrating the main processing sections.

3.3 Algorithm Input

3.3.1 Primary Sensor Data

Table 3 lists the primary sensor data used by the aerosol retrieval, including calibrated and geolocated PATMOS-x AVHRR + HIRS 'Level-2B' reflectance at 3 channels from AVHRR sensor, geolocation information, and sensor data quality flags. Here we also

include channel 3a even though this channel is only available for the AVHRR sensors onboard NOAA-15 and follow-on satellites.

Table 3: Primary AVHRR sensor L2B input data for aerosol retrieval.

Name	Type	Description	Dimension (spatial resolution)
Ch1 reflectance	Input	Calibrated channel 1 reflectance at 0.63μm	orbital grid (0.1° x 0.1°)
Ch2 reflectance	Input	Calibrated channel 2 reflectance at 0.83μm	orbital grid (0.1° x 0.1°)
Ch3a reflectance	Input	Calibrated channel 3a reflectance at 1.61μm	orbital grid (0.1° x 0.1°)
Latitude	Input	Grid latitude	orbital grid (0.1° x 0.1°)
Longitude	Input	Grid longitude	orbital grid (0.1° x 0.1°)
Solar geometry	Input	Solar zenith and azimuth angles	orbital grid (0.1° x 0.1°)
View geometry	Input	View zenith and azimuth angles	orbital grid (0.1° x 0.1°)
QC flags	Input	Quality control flags with level 2B data	orbital grid (0.1° x 0.1°)

3.3.2 Ancillary Data

The aerosol algorithm requires two ancillary input datasets: 1) Cloud probability and surface types input (Table 4) from cloud retrieval system in the AVHRR+HIRS PATMOS-x Data Processing System (APDPS). 2) Static look-up tables (LUTs) for atmosphere (molecular + aerosol + surface)(Table 5).

Table 4: Ancillary input data from the AVHRR+HIRS PATMOS-x L2B product and sea ice concentration CDR.

Name	Type	Description	Dimension (spatial resolution)
Cloud probability	Input	PATMOS-x level 2B data	orbital grid (0.1° x 0.1°)
Land/water info.	Input	PATMOS-x level 2B data	orbital grid (0.1° x 0.1°)
Sunglint info.	Input	PATMOS-x level 2B data	orbital grid (0.1° x 0.1°)
Snow/ice info.	Input	PATMOS-x level 2B data	orbital grid (0.1° x 0.1°)

Table 5: Look-up table (LUT) input data.

Name	Type	Description	Dimension
Ch1 LUT	Input	TOA apparent reflectance at 0.63μm channel as function of solar zenith angle, relative azimuth angle, view zenith angle, and aerosol optical thickness	15 x 19 x 15 x 7
Ch2 LUT	Input	TOA apparent reflectance at 0.83μm channel as function of solar zenith angle, relative azimuth angle, view zenith angle, and aerosol optical thickness	15 x 19 x 15 x 7
Ch3a LUT	Input	TOA apparent reflectance at 1.61μm channel as function of view zenith angle, relative azimuth angle, solar zenith angle, and aerosol optical thickness	15 x 19 x 15 x 7

3.3.3 Derived Data

Not applicable

3.3.4 Forward Models

The non-vector version of 6S (Second Simulation of the Satellite Signal in the Solar Spectrum) radiative transfer model or code (Vermote et al., 1997a, b) are used to produce the retrieval look-up tables (LUTs) in advance.

3.4 Theoretical Description

The feasibility of aerosol retrieval from satellite-observed radiances is based on the fact that these reflectances are affected by the physical and chemical properties of aerosols (Ackerman, 1997). The AVHRR algorithm retrieves the aerosol optical thickness from reflectance (or radiances) observed in the AVHRR visible and near infrared channels. The assumption is that the contributions of the molecular atmosphere and ocean surface can be accurately computed, and the aerosol can be represented by an averaged oceanic aerosol model based on AERONET observations (see Holben et al., 1998, 2001).

3.4.1 Physical and Mathematical Description

a) Strategy

The ocean/water AOT retrieval algorithm is based on a look-up table approach. A set of top-of-atmosphere (TOA) apparent reflectance (including contributions from molecular, aerosol, and surface) are pre-computed for each AVHRR retrieval channel by using a radiative transfer model (RTM), such as 6S model (Vermote et. al., 1997b), and stored in LUTS. For each retrieval channel, TOA reflectance from the LUT is compared with the observed reflectance through interpolation for a given solar-view geometry and a set of

aerosol optical thickness to find the best match. The corresponding AOT for the best match is the retrieval solution. The AOT retrieval algorithm has been illustrated schematically in the above Figure 1.

b) Aerosol Model

Aerosol model is represented by the combination of a fine lognormal and a coarse lognormal mode given in Eq. (8).

$$\frac{dN(r)}{d\ln r} = \sum_{i=1}^{2} \frac{N_0}{\sqrt{2\pi}\ln\sigma_{g,i}} \exp\left[-\frac{\left(\ln r - \ln r_{g,i}\right)^2}{2\left(\ln\sigma_{g,i}\right)^2} \right] \quad (8)$$

where $N(r)$ is the number density corresponding to particles of radius within (r, $r+dr$), $r_{g,i}$ is the geometric mean radius, and $\sigma_{g,i}$ is the associated standard deviation of the radius. The fine and coarse modes are adopted from AERONET observation and summarized in Table 6 along with their microphysical properties. These microphysical properties were determined from the validation of the AVHRR aerosol retrievals against the AERONET observations (see Zhao et al., 2002, 2004).

Table 6: Microphysical properties of ocean aerosol model used in the AOT algorithm, including geometric mean radius (r_g), standard deviation (σ_g), and refractive index.

Aerosol Model	r_g	σ_g	**Refractive index at retrieval wavelength (μm)**		
			0.63	0.83	1.61
Fine Mode	0.044	1.96	1.45 - 0.005i	1.45 – 0.007i	1.45 – 0.005i
Coarse Mode	0.370	2.370	1.45 - 0.005i	1.45 – 0.007i	1.45 – 0.005i

c) Modeling TOA reflectance over ocean

Following the 6S radiative transfer model (Vermote, 1997a), the spectral reflectance at the satellite level (ρ_{toa}) is a combination of radiation from the surface (ρ_{surf}) and the atmosphere (ρ_{atm}) due to reflection, scattering by molecules and aerosols and absorption by aerosols and gases as shown in Eq. (9):

$$\rho_{toa} = \rho_{atm} + \rho_{surf} \quad (9)$$

Here the spectral (or channel) index is omitted for simplicity. To facilitate the calculation of atmospheric reflection with varying gaseous amount and surface pressure, gas absorption, aerosol and Rayleigh scattering are decoupled by assuming a three-layer vertical model, where ozone and other minor absorbing gases (O_2, CO_2, N_2O, CH_4) (except water vapor) is on the top layer, molecular scattering in the middle layer, and the well-mixed aerosol and water vapor at the bottom layer. Without the consideration of

interaction between aerosol and Rayleigh scattering, the atmospheric contribution to TOA reflectance is computed as:

$$\rho_{atm} = T^{O_3} T^{og} \left[(\rho_{R+A} - \rho_R(P_0)) T^{\frac{1}{2}H_2O} + \rho_R(P) \right] \quad (10)$$

where,

T^{O_3} is ozone transmittance,

T^{og} is the gas transmittance other than ozone and water vapor,

T^{H_2O} is the total column water vapor transmittance,

$T^{\frac{1}{2}H_2O}$ is the half column water vapor transmittance,

ρ_{R+A} is the path reflectance by aerosols and molecules at standard pressure,

$\rho_R(P_0)$ is the Rayleigh reflectance from molecules at standard pressure = 1atm,

$\rho_R(P)$ is the Rayleigh reflectance from molecules at the actual pressure .

By given the profiles of atmosphere (e.g., middle-latitude summer), greenhouse gases, aerosols (including aerosol model), these terms and the atmospheric reflectance (ρ_{atm}) are calculated directly from 6S code.

The reflectance of ocean surface is modeled as Lambertian dark water surface with diffuse glint correction according to Breon (1993). The Lambertian surface reflectance is calculated directly from 6S code. The surface albedos used are 0.02, 0.01, and 0.002 respectively for 0.63, 0.83, and 1.61μm retrieval channels. The diffuse glint correction is calculated separately following Eq (21) in Breon (1993) and applied to the 6S modeling to obtain ρ_{surf} . Combined ρ_{atm} and ρ_{surf} are used to determine ρ_{toa} from Eq. (9) and stored in LUTs for retrieving use.

3.4.2 Data Merging Strategy

The AOT retrievals are performed for each daily orbital observation of AVHRR in a 0.1°x0.1° resampled grid, which is determined by the input PATMOS-x level-2B radiance. The final AVHHR daily AOT CDR product is obtained by merging daily orbital retrievals of multi-platforms for a given grid (0.1°x0.1°) and day through averaging. The gridded daily AOT CDR in a month is further averaged to obtain monthly AOT CDR.

3.4.3 Numerical Strategy

The retrieval values fall in between -0.2 and 5.0 (-0.2 ≤ AOT ≤5.0) are considered as the valid values. We permitted small negative AOT values in order to avoid an arbitrary negative bias at the low AOT end (due to the uncertainty associated with our uniform assumption of surface perturbation for all global water surfaces) in long term statistics. This means in very clean conditions over a calm ocean surface, the algorithm cannot determine if the AOT = 0, 0.2 or -0.2 since the uncertainty due to the ocean surface perturbation assumption obscured the aerosol information if AOT is small. If we eliminate

all the negative numbers and keep all the positive numbers, we introduce an artificial bias. Thus, we allow the small negative retrievals. To interpret these: If you are calculating long-term statistics, simply add the negatives into the mix and don't worry about them. If you were looking at individual retrievals then count negative retrievals as 'very clean'. You could force them to be AOT = 0, for example. It really depends on the application. However, these small negative AOT values are valid retrievals and do contain information. Missing values (-999.0) are put in the grids without successful retrievals or the retrieved values fall beyond the valid range.

3.4.4 Calculations

The retrieval is performed for 1) solar zenith angle $\theta_s < 70^o$ and view zenith angle $\theta_v < 60^o$ to minimize atmospheric curvature effects; 2) glint angle $\eta > 40^o$ to avoid sun glint contamination; 3) relative azimuth angle $\phi_{sv} > 90^o$ (the anti-solar side of satellite orbit) to include only back scattering. For a given orbital grid (observing geometry), the model TOA apparent reflectance in LUTs for a retrieval channel is compared with observations to determine the optimal solution through interpolation. The AOT value corresponding to the best match of apparent reflectance is the final retrieved AOT for this pixel or grid. The retrieval is performed according to two loops: latitude and longitude loops. For the orbital grids that do not meet the retrieval conditions, a fill value (-999.0) is provided. The orbital grid level AOT retrievals are performed in 0.1^ox0.1^o equal angle grid and output in a 2-D array (latitude x longitude). This gridded daily orbital AOT product will be further averaged to produce daily mean and monthly mean AOT products on the same grids, which are served as the final CDR AOT products.

3.4.5 Look-Up Table Description

As the backbone of AVHRR AOT retrieval, LUTs for the three retrieval channels are generated with the non-vector version of 6S radiative transfer code. The TOA apparent reflectance for a set of solar-view geometries (view zenith angle, relative azimuth angle, and solar zenith angle) and aerosol optical thickness are pre-calculated for the selected aerosol mode given in Section 3.4.1 for the three retrieval channels and are stored in three 4-dimension tables, respectively. Reflectance contribution of molecular, aerosol, and surface are all included in the stored reflectance. The middle latitude summer atmosphere and Lambertian dark water surface with diffuse glint correction on aerosol phase function are used for generating LUT. The surface albedos are set to 0.02, 0.01, and 0.002 in the 6S input cards for AVHRR 0.63, 0.83, and 1.61μm channels, respectively, for the generation of LUTs. The arguments and dimensions of the LUTs are given in Table 7. The corresponding 7 AOT bin values at 0.55μm (needed for 6S input card) for the aerosol model used are 0.000, 0.164, 0.328, 0.656, 0.984, 1.311, and 1.638.

Table 7: Arguments and dimensions of three LUTs.

Argument		Dimension	Bins
View zenith angle (o)		15	0.0, 6.0, 12.0, 18.0, 24.0, 30.0, 36.0, 42.0, 48.0, 54.0, 60.0, 66.0, 72.0, 78.0, 84.0
Relative azimuth angle (o)		19	0.0, 10.0, 20.0, 30.0, 40.0, 50.0, 60.0, 70.0, 80.0, 90.0, 100.0, 110.0, 120.0, 130.0, 140.0, 150.0, 160.0, 170.0, 180.0
Solar zenith angle (o)		15	0.0, 6.0, 12.0, 18.0, 24.0, 30.0, 36.0, 42.0, 48.0, 54.0, 60.0, 66.0, 72.0, 78.0, 84.0
AOT	at 0.63μm channel	7	0.000, 0.147, 0.294, 0.588, 0.882, 1.176, 1.470
	at 0.83μm channel	7	0.000, 0.113, 0.226, 0.452, 0.678, 0.904, 1.130
	at 1.61μm channel	7	0.000, 0.082, 0.164, 0.328, 0.492, 0.656, 0.820

3.4.6 Parameterization

Not Applicable

3.4.7 Algorithm Output

The orbital grid level retrievals are performed in the same 0.1°x0.1° equal angle grid (total 1800 x 3600 = 6480000 grids over the globe) as the input L2B reflectance and write to output accordingly in the HDF format for both channels 1 and 2 of AVHRR. The daily orbital output product for AVHRR channel 1 from different satellite platforms will be further averaged to produce the daily mean and monthly mean products on the same 0.1°x0.1° grids and in NetCDF-4 format, which are served as CDR AOT products. The size of one daily orbital output file is between about 25 and 800KB, one daily mean product file is about 26MB, and one monthly mean product file is about 26MB. The summary of the three output products are provided in Tables 8, 9, and 10, respectively.

Table 8: Daily orbital AOT product in HDF format.

Name	Type	Description	Spatial Resolution
latitude	output	Latitude of grid center (1800)	0.1° x 0.1°
longitude	output	Longitude of grid center (3600)	0.1° x 0.1°
aot1_Final	output	Mean channel 1 AOT (6480000)	0.1° x 0.1°
aot2_Final	output	Mean channel 2 (or 3a) AOT (* this is an optional output) (6480000)	0.1° x 0.1°

Table 9: Daily mean CDR AOT product in NetCDF-4 format.

Name	**Type**	**Description**	**Spatial Resolution**
latitude	output	Latitude of grid center (1800)	0.1^o x 0.1^o
longitude	output	Longitude of grid center (3600)	0.1^o x 0.1^o
aot1	output	Daily mean channel 1 AOT (3600x1800)	0.1^o x 0.1^o

Table 10: Monthly mean CDR AOT product in NetCDF-4 format.

Name	**Type**	**Description**	**Spatial Resolution**
latitude	output	Latitude of grid center (1800)	0.1^o x 0.1^o
longitude	output	Longitude of grid center (3600)	0.1^o x 0.1^o
aot1	output	Monthly mean channel 1 AOT (3600x1800)	0.1^o x 0.1^o

4. Test Datasets and Outputs

4.1 Test Input Datasets

The algorithm is used to produce aerosol CDR from long-term operational AVHRR observations. Thus, the current version (v6.0) of long-term PATMOS-x AVHRR _ HIRS level-2B gridded orbital data (in a spatial resolution of 0.1^o x 0.1^o) from 1981 to 2022 are used as input data. Current version 4/revision 0 (v04r00) replaces the previous version 3 (v03r00). Version 3 (v03r00) was produced using the same algorithm for the input from old version (v5.3) of PATMOS-x AVHRR level-2B gridded orbital data. For the versions 4, 3, and 2, the AOT retrieval system is independent from the APDPS and only the output parameters from the APDPS are used as the input of the AOT retrieval system, which greatly reduces the complicity of the retrieval system and the processing time comparing to the version 1. It also provides a good example of how to produce CDR from FCDR. Specifically, in version 4, the PATMOS-x AVHRR+HIRS level-2B data (or FCDR) are produced by the APDPS and the radiances (or reflectances) used for the retrieval are re-calibrated in the APDPS by using the new calibration coefficients. The new calibration coefficients are obtained offline by comparing the match-ups between accurate MODIS radiance and AVHRR radiances (Heidinger et al., 2002, 2010; Molling et al., 2010). The cloudy probability (cpb) is determined in the APDPS using a naïve Bayesian cloud detection technique (see Heidinger et al., 2012) for each grid by using the 3x3 pixels around it. The clear-sky radiance (in a spatial resolution of 0.1^o x 0.1^o) is defined for those grids with cpb ≤ 1% and is used by the aerosol retrieval algorithm. Please refer to the website (https://www.ncei.noaa.gov/products/climate-data-records) of the NCEI CDR program for more information on the APDPS.

4.2 Test Output Analysis

4.2.1 Reproducibility

Using the IOC retrieval codes written in IDL (which is delivered to the CDR program along with this C-ATBD) and the test input data mentioned in the above section 4.1, the AOT CDR products should be able to be reproduced to the level of machine rounding error on a Linux computer system.

An example of daily orbital AOT product (at 0.63μm channel) for January 1, 2005 is plotted in Figure 2 for NOAA-16/AVHRR ascending node. 16 AOT swaths correspond to 16 satellite orbits in a day. The daily orbital data of NOAA-15, -16, -17, and -18 for the same day are averaged to form daily mean AVHRR AOT CDR as shown in Figure 3. The daily mean AOT CDRs are further averaged to form the monthly mean AOT CDR as shown in Figure 4 for the January 2005.

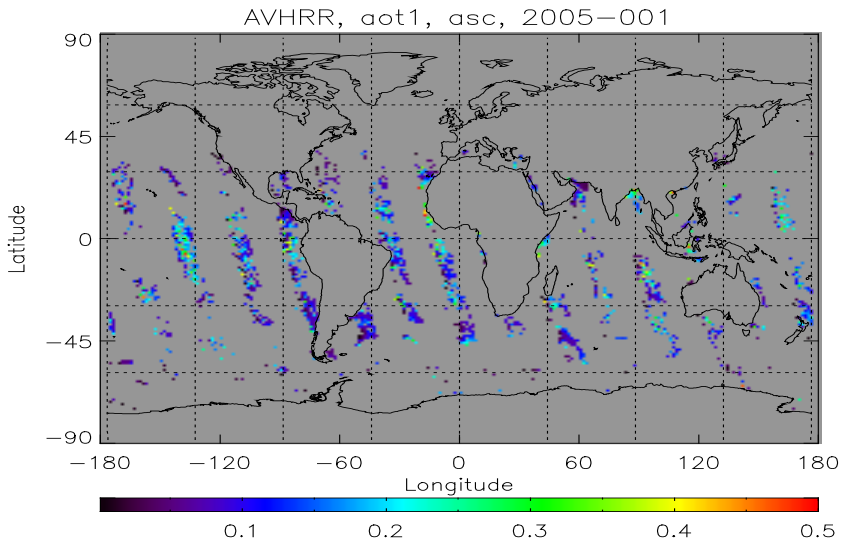

Figure 2: Example of daily orbital AOT (at 0.63μm channel) product for NOAA-16/AVHRR ascending node on January 1, 2005.

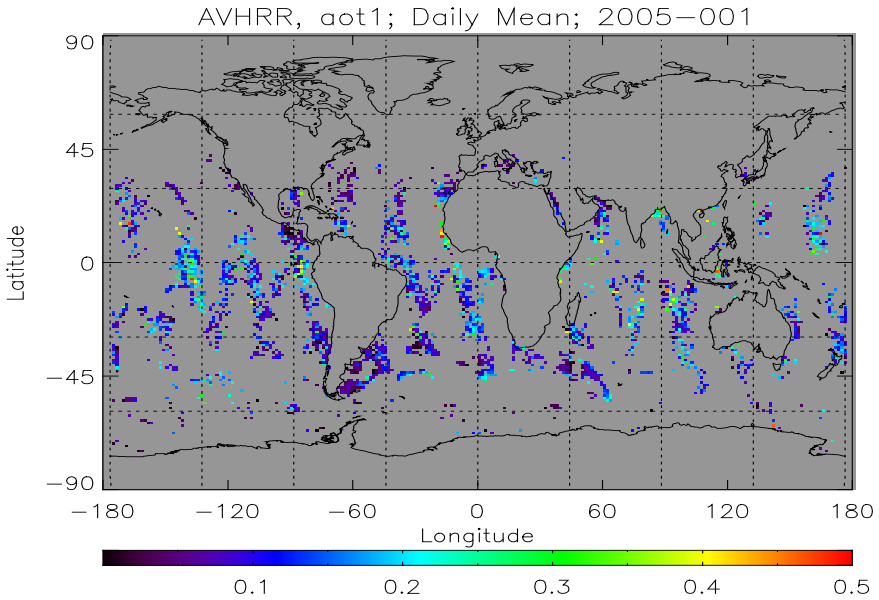

Figure 3: Example of daily mean AOT (at 0.63μm channel) CDR product for January 1, 2005 by averaging the daily orbital AOT from the AVHRR of NOAA-15, -16, -17, and -18.

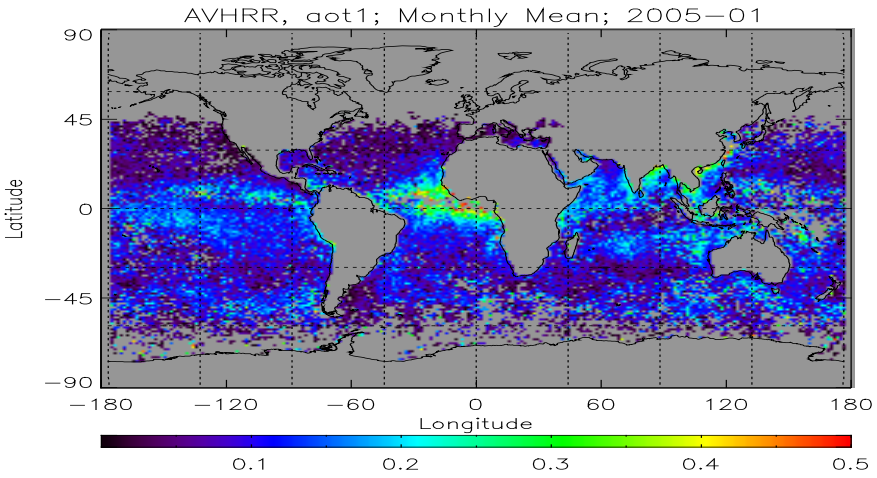

Figure 4: Example of monthly mean AOT (at 0.63μm channel) CDR product for January 2005.

Example of AOT time series for our monthly product is shown in Figure 5 for the versions 1 2, and 3. The difference among the three versions is mainly due to the difference in cloud screening (see Zhao et al., 2013, 2016). Version 3 compares better to the Terra/MODIS AOT product (which is also shown in Figure 5) than the other two previous versions.

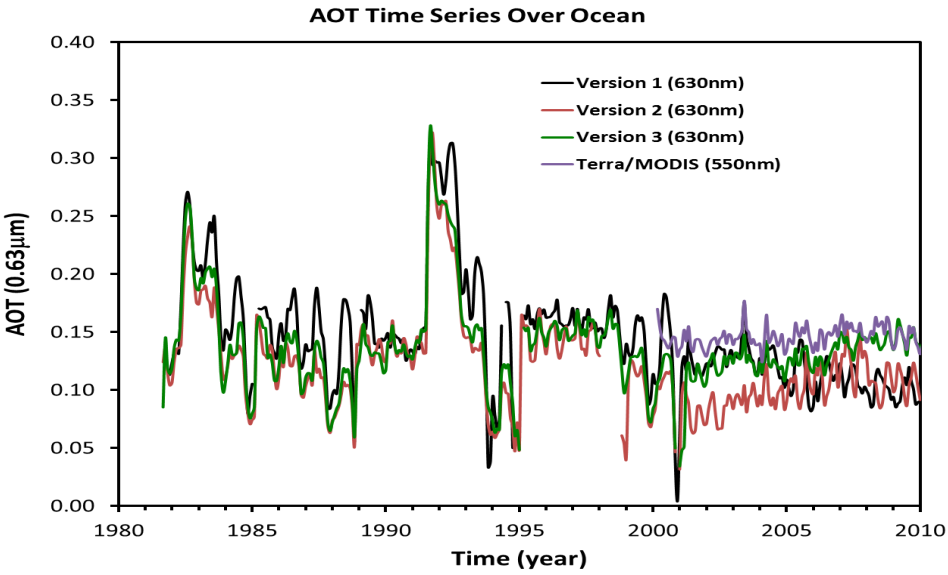

Figure 5: Example of AVHRR AOT CDR (0.63μm) time series for the versions 1, 2, and 3 and their comparison with Terra/MODIS AOT (0.55μm).

Figure 6 is an example showing the AOT distributions on the north polar latitudes in July 2019 for version 3 and 4, respectively. Spurious high AOT values over polar seas in version 3.0 have been removed in the version 4.0 due to better cloud detection and screening in the input data of PATMOS-x AVHRR+HIRS cloud CDRs.

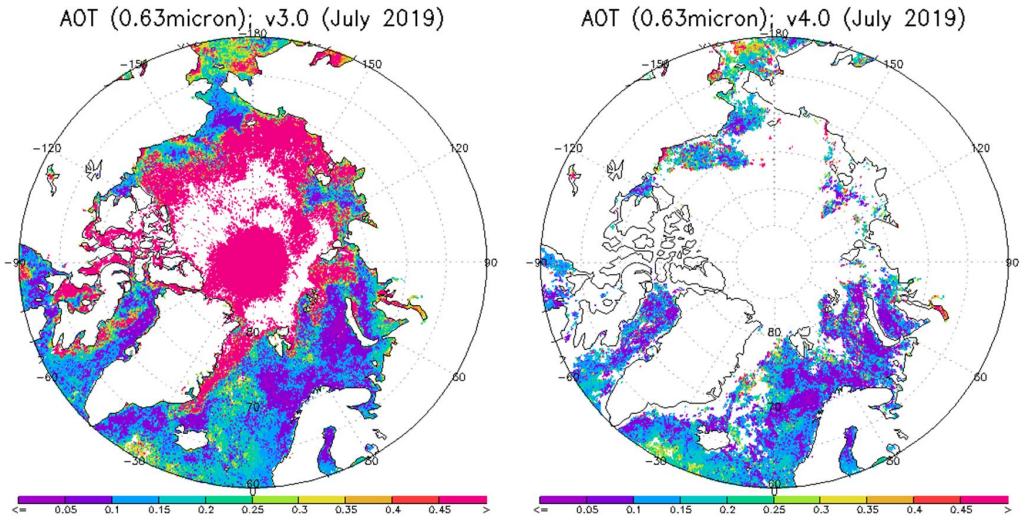

Figure 6: AOT distribution on the north polar latitudes in July 2019 for version 3.0 (left panel) and version 4.0 (right panel).

Comparison of AOT time series for the global monthly product of version 3.0 and version 4.0 is shown in Figure 7. AOT values of version 4.0 is slightly lower than that of version 3.0 before 2016 but become somewhat larger than version 3.0 afterward. The strange spikes in summer of 2018 and 2019 in version 3.0, which are associated with the spurious high values over polar oceans (see Figure 6) due to residual cloud contamination, are removed in version 4.0 due to better cloud detection and screening in the input data of PATMOS-x AVHRR+HIRS cloud CDRs.

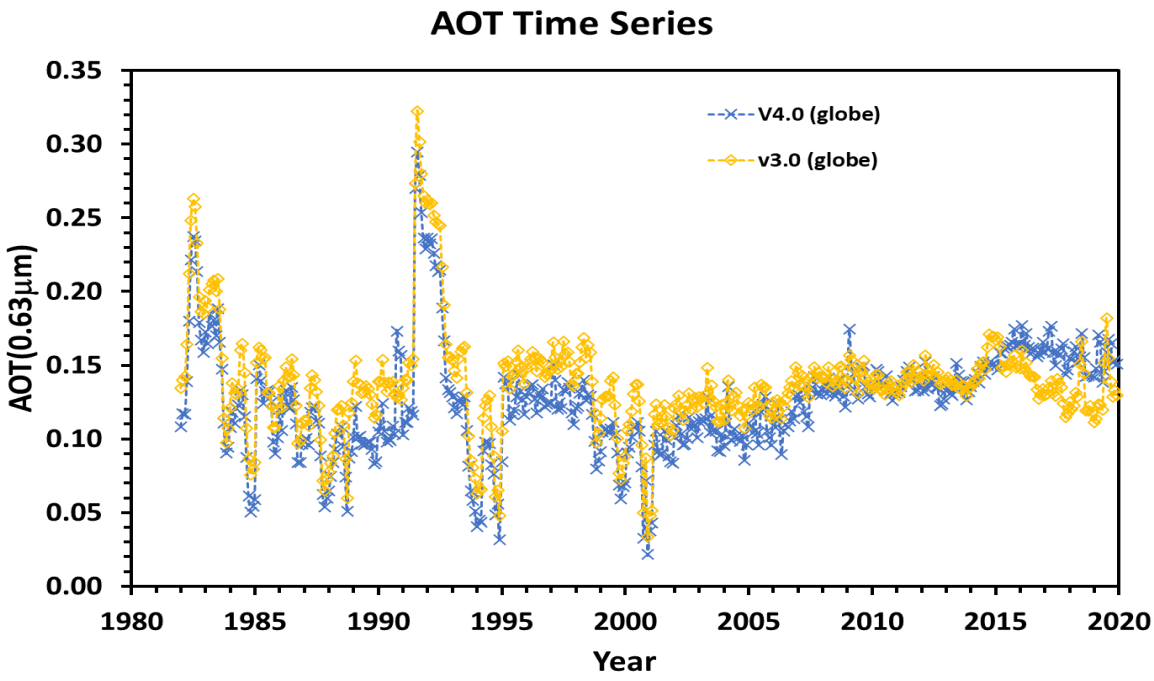

Figure 7: Comparison of global AVHRR AOT CDR (0.63µm) time series between version 3.0 (yellow dashed line) and version 4.0 (blue dashed line).

4.2.2 Precision and Accuracy

The precision and accuracy of AVHRR AOT CDR products are determined through validation of comparing with ground truth (such as AERONET observations) and inter-satellite comparison. The validation and evaluation is a continuous effort in the development of the retrieval algorithm so that it will be updated from time to time. The obtained accuracy is 0.05 with a precision of about 0.09.

4.2.3 Error Budget

The error budget of AVHRR AOT CDR products is summarized in Table 11. The results are based on AERONET validation. Since the selected AERONET stations in the validation are over islands so that the validation results represent the coastal marine condition. In the future, AERONET observations over ships will be collected for our validation so that the algorithm performance can be further assessed for remote marine condition.

Table 11: Systematic and random errors for the AVHRR AOT retrieval based on surface AERONET validation.

AVHRR Channel	**Systematic Errors**			**Random Error (±)**
	Minimum (τ = 0.00)	Mean (τ = 0.15 at λ_1) (τ = 0.11 at λ_2)	Maximum (τ = 1.00)	
λ_1=0.63μm	0.031	0.030	0.024	0.113
λ_2=0.83μm	0.032	0.032	0.035	0.103

5. Practical Considerations

5.1 Numerical Computation Considerations

a. LUT is used for increasing speed.

b. Linear interpolation of LUT values.

5.2 Programming and Procedural Considerations

a. Retrieval is performed on orbital grid (0.1^{o}x0.1^{o}) and output on the same grids in HDF format. Then, the orbital grid level retrievals are averaged to both daily and monthly products on the same grids in NetCDF format.

b. Calibrated and geo-located reflectances, cloudy probably from the cloud mask (CM) and snow/ice mask must be available before aerosol retrieval.

c. Program modules are used to ease modification and upgrades.

d. The jobs are run on numerous computers via Bourne shell scripts to speed up the execution and data production in a research oriented computing environment. The batch file is broke up into smaller batch files which are then launched on numerous nodes.

5.3 Quality Assessment and Diagnostics

The following flags or variables will be produced:

- Missing/No data.

5.4 Exception Handling

The quality control flags for aerosol retrieval will be checked and inherited from the flagged PATMOS-x AVHRR+HIRS Level-2B input data, including bad sensor input data, missing sensor input data and validity of each aerosol channel; and will be checked and inherited from the PATMOS-x cloud mask at each pixel for clear, possibly clear, cloud and possibly cloudy.

The algorithm does checks for conditions not favorable for aerosol retrieval, such as snow/ice pixel, glint area, and viewing geometry.

5.5 Algorithm Validation

AERONET observations (see Holben et al., 1998, 2001) are commonly used as ground truth for the validation of satellite aerosol retrievals (e.g., Hsu et al., 1999; Chu et al., 2002; Remer et al., 2002; Torres et al., 2002; Zhao et al., 2002, 2004; Kahn et al., 2005). We have selected 9 AEONET island stations which cover the major regimes of global oceanic aerosol characteristics as our validation sites. Three years (1998-2000) of quality

assured level 2 AERONET aerosol optical thickness observations (temporally averaged within ±1-hour window around AVHRR overpass) are used as our ground truth and collocated with AVHRR aerosol retrievals (spatially averaged in a 100x100 km box with an inner circle of about 25km in radius excluded). Total 599 match-up points have been found and used for the validation statistics. Detailed validation approach and results can be found in Zhao et al. (2002, 2004). The validation results for the retrievals at 0.63 and 0.83μm are shown in Figure 8.

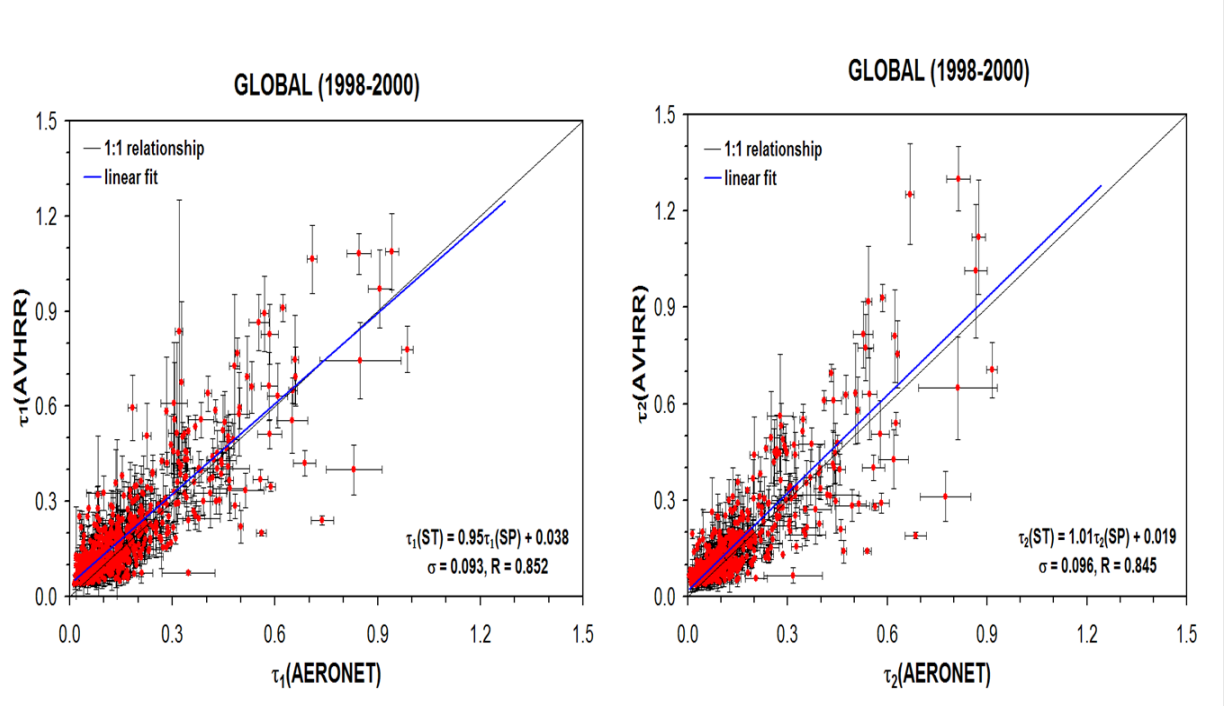

Figure 8: Scatter plots of AVHRR retrievals versus AERONET observations for 0.67μm channel (left panel) and 0.83μm channel (right panel).

For version 4.0, AOT CDR is also validated using the MARITIME AEROSOL NETWORK (MAN) data (Smirnov et al., 2009). Five years (2015-2019) of quality assured level 2 MAN data product is collocated with the mean value of the AVHRR AOTs within a 0.5° by 0.5° box around the ship location considering the spatial resolution of AVHRR AOT is 0.1° by 0.1°. Total 1556 match-up points have been found and used for the validation statistics. The validation result is shown in Figure 9.

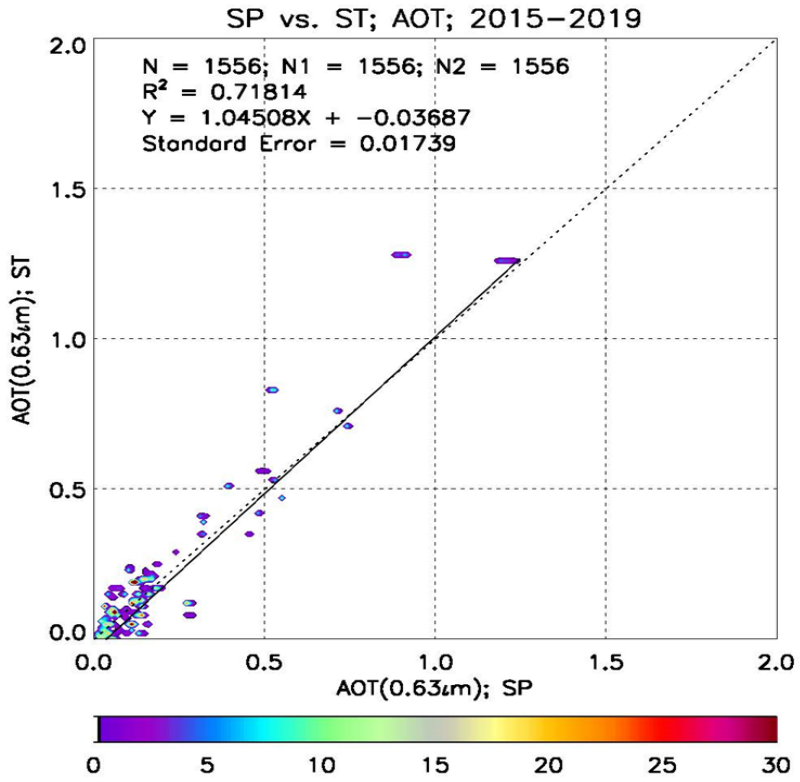

Figure 9: Scatter plots of AVHRR retrievals (ordinate) versus MAN observations (abscissa) for 0.63μm channel.

5.6 Processing Environment and Resources

The processing system configuration in a research oriented computing environment is listed below:

- CPU: Intel (R) Xeon ® X5680 @ 3.33GHz, 16.7GB memory
- Operating system: GNU/Linux; Red Hat 4.4.6-4
- Programming languages: IDL and Bourne Shell Script
- Compilers: IDL Version 8.2.3
- External libraries: NetCDF 4.3.0
- Total CPU time (for one year run): ~1328 minutes
- Total wall clock time (for one year run): ~1440 minutes

- Working space (for 41 years 1982-2022 data): Input data 9.6TB; Daily AOT CDR product 329GB; Monthly AOT CDR product 12.4GB.

6. Assumptions and Limitations

The following sections describe the current limitations and assumptions in the current version of the AVHRR AOT retrirval system.

6.1 Algorithm Performance

Assumptions have been made in developing and estimating the performance of the current retrieval algorithm. The following list contains the current assumptions and proposed mitigation strategies.

- Aerosol has globally fixed optical properties;
- Aerosol is in spherical shape and in bi-mode lognormal distribution;
- It is vertically well-mixed;
- Surface is dark and Lambertian with a diffuse glint correction;
- PATMOS-x cloud mask and accurate clear-sky reflectance are available;
- Sea ice concentration monthly CDR are available;
- Atmospheric state is fixed;
- Perform retrieval only in daytime and over dark ocean surface;
- Does not account for bidirectional reflectance over ocean.

6.2 Sensor Performance

It is assumed that the satellite sensor will meet its current specifications. However, the AOT CDR performance will be dependent on the following instrument characteristic:

- Properly inter-calibrated and geo-located sensor radiances in AVHRR channels 1-5.

7. Future Enhancements

The following listed items are our planned research and improvement on our retrieval and data processing.

7.1 Enhancement 1

Continue the validation of the retrieval for more years and more conditions.

7.2 Enhancement 2

Account for bidirectional reflectance over ocean

7.3 Enhancement 3

Extended the retrieval to new satellite sensors (such as JPSS/VIIRS) and the dark land surface.

8. References

Ackerman, S. A. (1997). Remote sensing aerosols using satellite infrared observations. J. Geophys. Res. 102, 17069–17079.

Breon, F. M. (1993). An analytical model for the cloud free atmosphere/ocean system reflectance. Remote Sens. Environ., 43, 179-192.

Chan, P. K., X. Zhao, and A. K. Heidinger (2013), Long-term aerosol climate data record derived from operational AVHRR satellite observations, Dataset Paper in Geosciences, Article ID 140791, 2013.

Chu, D. A., Y. J. Kaufman, C. Ichoku, L. A. Remer, D. Tanre, B. N. Holben (2002). Validation of MODIS aerosol retrieval over land. Geophys. Res. Lett., 29, doi:10.1029/2001GL013205.

Heidinger, A.K., Cao, C. and Sullivan, J.T. (2002). Using moderate resolution imaging spectrometer (MODIS) to calibrate advanced very high resolution radiometer reflectance channels. Journal of Geophys. Res., 107, 4702, doi:10.1029/2001JD002035.

Heidinger, A.K., Straka III, W.C., Molling, C.C., Sullivan, J.T. and Wu, X. (2010). Deriving an inter-sensor consistent calibration for the AVHRR solar reflectance data record. International Journal of Remote Sensing, 31, 6493-6517.

Heidinger, A. K., Evan, A. T., Foster, M. J. and Walther A. (2012). A naïve Bayesian cloud-detection scheme derived from CALIPSO and applied within PATMOS-x, Journal of Applied Meteorology and Climatology, 51(6), 1129–1144.

Heidinger, A. K., M. J. Foster, A. Walther, and X. Zhao (2014), The Pathfinder Atmospheres Extended (PATMOS-x) AVHRR Climate Data Set, Bull. Amer. Meteorol. Soc., 95, 909-922.

Holben B.N., et al. (1998). AERONET - A federated instrument network and data archive for aerosol characterization. Rem. Sens. Environ., 66, 1-16, 1998.

Holben, B.N., et al. (2001). An emerging ground-based aerosol climatology: Aerosol Optical Depth from AERONET. J. Geophys. Res., 106, 12,067-12,097.

Hsu, N. C., J. R. Herman, O. Torres, B. N. Holben, D. Tanre, T. F. Eck, A. Smirnov, B. Chatenet, and F. Lavenu (1999). Comparisons of the TOMS aerosol index with Sun-photometer aerosol optical thickness: Results and applications, J. Geophys. Res., 104, 6269-6279.

Kahn, R., B. Gaitley, J. Martonchik, D. J. Diner, C. A. Crean, and B. Holben (2005). Multiangle Imaging Spectroradiometer (MISR) global aerosol optical depth validation based on 2 years of coincident Aerosol Robotic Network (AERONET) observation. J. Geophys. Res., 110, doi:10.1029/2004JD004706.

Mei, L. L., Burrows, J. P., Zhao, X.-P., Vountas, M., Rozanov, V., Lelli, L., Xinwu Li, X., Guo, H., Nakoudi, K., Ritter, C., and Edebor, A. A. An analysis of AOT above the ocean in the Arctic observed from space: a reducing trend from 1981 to 2019. In preparation.

Molling, C.C., Heidinger, A.K., Straka III, W.C. and Wu, X (2010). Calibrations for AVHRR channels 1 and 2: review and path toward consensus. International Journal of Remote Sensing, 31(24), 6519-6540.

Remer, L. A., D. Tanre, Y. J. Kaufman, C. Ichoku, S. Mattoo, R. Levy, D. A. Chu, B. N. Holben, O. Dubovik, A. Smirnov, J. V. Martins, R-R. Li, Z. Ahmad (2002). Validation of MODIS aerosol retrieval over ocean. Geophys. Res. Lett., 29, doi:10.1029/2001GL013204.

Smirnov, A., Holben, B. N., Slutsker, I., Giles, D. M., McClain, C. R., Eck, T. F., Sakerin, S. M., Macke, A. , Croot, P., Zibordi, G., Quinn, P. K., Sciare, J., Kinne, S., Harvey, M., Smyth, T. J., Piketh, S., Zielinski, T., Proshutinsky, A., Goes, J. I., Nelson, N. B., Larouche, P., Radionov, V. F., Goloub, P., Krishna Moorthy, K., Matarrese, R., Robertson, E. J. & Jourdin, F. (2009). Maritime Aerosol Network as a component of Aerosol Robotic Network. Journal of Geophysical Research, 114(D6), doi:10.1029/2008jd011257

Torres, O., P. K. Bhartia, J. R. Herman, A. Sinyuk, P. Ginoux, and B. Holben (2002). A long-term record of aerosol optical depth from TOMS observations and comparision to AERONET measurements, J. Atmos. Sci., 59, 398-413.

Vermote, E. F., D. Tanre, J. L. Deuze, M. Herman, and J. J. Morcrette (1997a). Second Simulation of the Satellite Signal in the Solar Spectrum, 6S: An overview. IEEE Trans. Geosci. Remote Sens., 35(3), 675-686.

Vermote, E. F. et al. (1997b). 6S User Guide, Version 2.

Zhao, X., L. L. Stowe, A. B. Smirnov, D. Crosby, J. Sapper, and C. R. McClain (2002). Development of a global validation package for satellite oceanic aerosol optical thickness retrieval based on AERONET observations and its application to NOAA/NESDIS operational aerosol retrievals. J. Atmos. Sci., 59, 294-312.

Zhao, X., O. Dubovik, A. B. Smirnov, B. N. Holben, J. Sapper, C. Pietras, K. J. Voss, and R. Frouin (2004). Regional Evaluation of an AVHRR two-channel aerosol retrieval algorithm. Journal of Geophys. Res., 109, D02204, doi:10.1029/2003JD003817.

Zhao, X., I. Laszlo, W. Guo, A. Heidinger, C. Cao, A. Jelenak, D. Tarpley, J. Sullivan (2008). Study of Long-term Trend in Aerosol Optical Thickness Observed from Operational AVHRR Satellite Instrument. J. Geophys. Res., 113, D07201, doi:10.1029/2007JD009061.

Zhao, T. X.-P., P. Chan, and A. K. Heidinger (2013). A Global Survey of the Effect of Cloud Contamination on the Aerosol Optical Thickness and Its Long-term Trend Derived from Operational AVHRR Satellite Observations, J. Geophys. Res., 118, 2849-2857, doi: 10.1002/jgrd.50278.

Zhao, T. X.-P., A. K. Heidinger, and Andi Walther (2016). Climatology Analysis of Aerosol Effect on Marine Water Cloud from Long-term Satellite Climate Data Records, Remote Sensing, 8(4), 300, doi: 10.3390/rs8040300.

Appendix A. Acronyms and Abbreviations

Acronym or Abbreviation	Definition
AACRS	AVHRR AOT CDR Retrieval System
AERONET	Aerosol Robotic Network
AOT	Aerosol Optical Thickness
APDPS	AVHRR PATMOS-x Data Processing System
AVHRR	Advanced Very High Resolution Radiometer
C-ATBD	Climate Algorithm Theoretical Basis Document
CDR	Climate Data Record
CDRP	CDR Program
CM	Cloud Mask
FCDR	Fundamental CDR
HDF	Hierarchical Data Format
IDL	Interactive Data Language
IOC	Initial Operating Capability
LUT	Lookup Table
L2B	Level-2B
MAN	Maritime Aerosol Network
NCDC	National Climatic Data Center
NCEI	National Centers for Environmental Information
NetCDF	Network Common Data Form
NOAA	National Oceanic and Atmospheric Administration
PATMOS-x	Pathfinder Atmospheres - Extended
QC	Quality Control
REDR	Reference Environmental Data Record
RTM	Radiative Transfer Model
SWIR	Shortwave Infrared
TOA	Top of Atmosphere
6S	Second Simulation of a Satellite Signal in the Solar Spectrum